Applied and Computational Mathematics | GFE GEMEINSCHAFTSLABOR FÜR ELEKTRONENMIKROSKOPIE | RWTH AACHEN UNIVERSITY

Subscale Inversion in Electron Probe Microanalysis Based on Deterministic Transport Equations

Gaurav Achuda, Tamme Claus, Silvia Richter and Manuel Torrilhon

Applied and Computational Mathematics
&
Central Facility for Electron Microscopy
RWTH Aachen University
Germany

funding by DFG Deutsche Forschungsgemeinschaft

Kinetic Transport Theory

- mesoscopic modeling framework for systems containing many similar micro-items

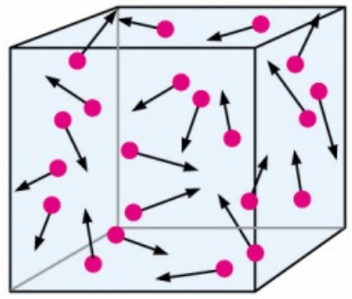
particle system


traffic flow


granular flow

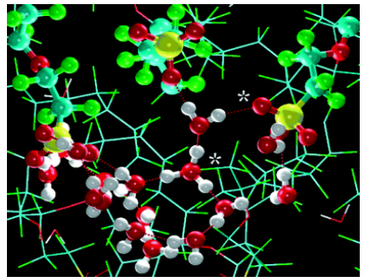
polymers / complex fluids


sprays / suspensions

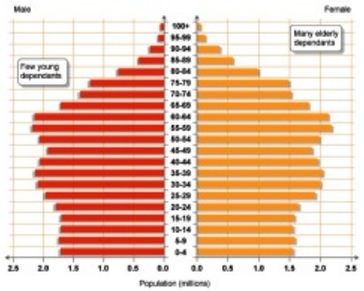

populations


rarefied gases

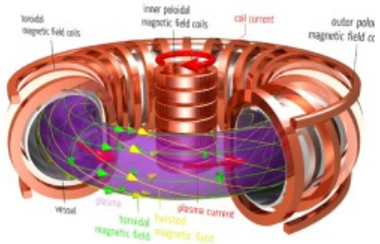
plasma flows


radiative transfer


bird flock


dust / soot propagation

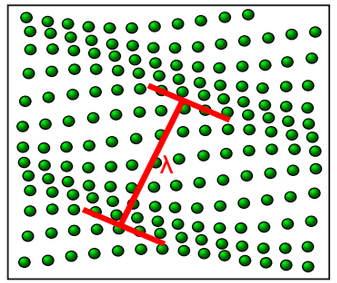

phonon dynamics

Fluid Dynamics

- from a physics perspective fluid dynamics may seem complete:

Microscopic Setting

particle positions and velocities $X_i(t),\ V_i(t)$

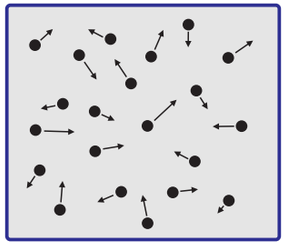

long wave length limit

Macroscopic Setting

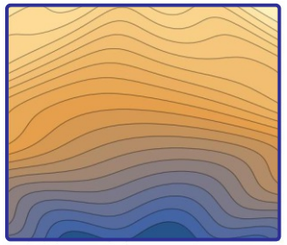

fluid dynamic fields: $\rho(\mathbf{x},t)$, $\mathbf{u}(\mathbf{x},t)$, $T(\mathbf{x},t)$, etc

- classical fundamental laws from first principles
- with particle interaction potential

$$\begin{aligned}\dot{X}_i(t) &= V_i(t)\\ m_i\dot{V}_i(t) &= \sum\nolimits_j F(\|X_i(t) - X_j(t)\|)\end{aligned}$$

- solved by molecular dynamics or Monte-Carlo simulations

- empirical laws based on observations
- Fourier's law of heat conduction $q_i = -\kappa\dfrac{\partial T}{\partial x_i}$
- law of Navier-Stokes for viscous stresses $\sigma_{ij} = -2\mu\dfrac{\partial u_{\langle i}}{\partial x_{j\rangle}}$
- solved by numerical methods for partial differential equations

The Need for Modeling

- various phenomena not covered by long wave length limit: non-gradient transport, cross-coupling effects, Knudsen boundary-layers, etc.
- particle dynamics/Monte-Carlo is inefficient (accurate, but slow), in particular for unsteady problems, large parameter space exploration and optimization problems
- mesoscopic moment models are as accurate as necessary, but not more, in order to ensure efficiency.
- ideally an hierarchical approach of cascading modelsis used to supplement existing simulations.

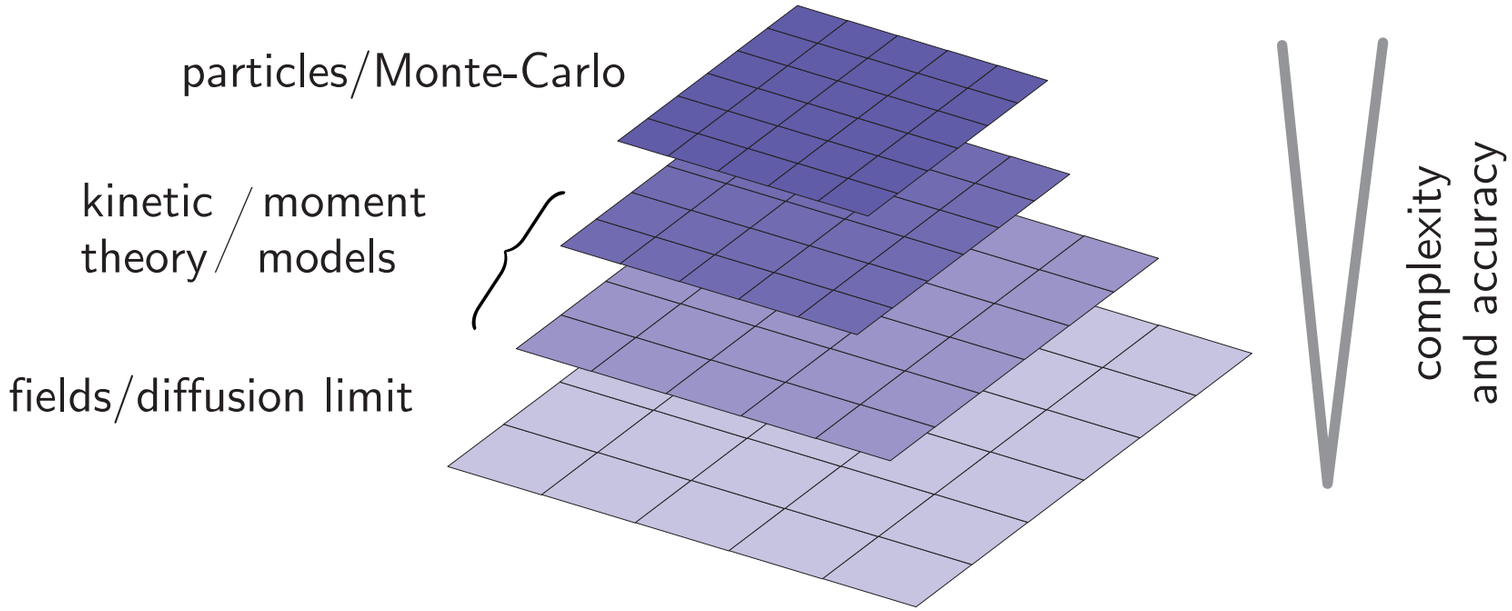

Radiative Transfer

Linear Transport

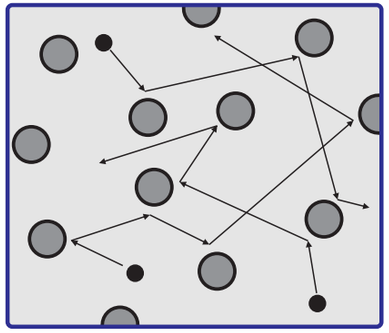

- particles interact with background material in scattering events
- no interaction between particles themselves
- long wave length limit corresponds to diffusion equation

- distribution f with value $f(\mathbf{x}, t, \mathbf{v})d\mathbf{v}$ gives the number density of particles with velocity in $[\mathbf{v}, \mathbf{v} + d\mathbf{v}]$
- linear kinetic equation for electrons interacting with background material

$$\frac{\partial}{\partial t} f + v_i \frac{\partial}{\partial x_i} f = -\int \underbrace{|v|\sigma(v \to v')\, f\,(x,t,v)}_{\text{scattering loss in phase space}}\, dv' + \int \underbrace{|v'|\sigma(v' \to v)\, f\,(x,t,v')}_{\text{scattering gain in phase space}}\, dv'$$

- crucial material parameter: differential cross section σ
- applications in nuclear engineering, electric arc simulations, medical radiation therapy, electron microscopy, etc

Steady State, Small Energy Changes

- consider steady state, i.e., time-independence, velocity $\boldsymbol{v}$ is split into energy ε and direction $\boldsymbol{\Omega}$
- velocity distribution is transformed into particle fluence $\psi(\mathbf{x}, \varepsilon, \boldsymbol{\Omega}) = \|v(\varepsilon, \boldsymbol{\Omega})\| f(\mathbf{x}, v(\varepsilon, \boldsymbol{\Omega}))$
- assuming small energy changes in scattering allows to derive the Continuous-Slowing-Down Approximation (CSDA)

$$\Omega_i \frac{\partial}{\partial x_i} \psi(\mathbf{x}, \varepsilon, \boldsymbol{\Omega}) = \underbrace{-\sigma_{\text{tot}}^{(\text{loss})}(\mathbf{x}, \varepsilon)\, \psi(\mathbf{x}, \varepsilon, \boldsymbol{\Omega})}_{\text{loss by directional scattering}} + \underbrace{\int_{\mathcal{S}^2} \sigma^{(\text{CSD})}(\mathbf{x}, \varepsilon, \boldsymbol{\Omega}' \cdot \boldsymbol{\Omega})\, \psi(\mathbf{x}, \varepsilon', \boldsymbol{\Omega}') d\boldsymbol{\Omega}'}_{\text{gain by directional scattering}} + \underbrace{\frac{\partial}{\partial \varepsilon} (S(\mathbf{x}, \varepsilon)\, \psi(\mathbf{x}, \varepsilon, \boldsymbol{\Omega}))}_{\text{energy gain in phase space}}$$

- general structure

$$-\partial_\varepsilon \left(S(\boldsymbol{x}, \epsilon) \psi(\boldsymbol{x}, \epsilon, \boldsymbol{\Omega})\right) + \boldsymbol{\Omega} \cdot \nabla_{\boldsymbol{x}} \psi(\boldsymbol{x}, \epsilon, \boldsymbol{\Omega}) = \mathcal{Q}\left[\psi(\boldsymbol{x}, \epsilon, \boldsymbol{\Omega})\right]$$

- material parameter: stopping power $S(\mathbf{x}, \varepsilon)$ derived from scattering cross-section σ, for example, Bethe-loss formula
- energy profile propagates towards lower energies

Linear Moment Models (P_N-Models)

- consider moments in direction, that is $\boldsymbol{\Omega} \in \mathcal{S}^2$ with fixed energy ε and position $\boldsymbol{x}$

$$\psi_{i_1 i_2 \cdots i_n}(x, \varepsilon) = \int_{\mathcal{S}^2} \Omega_{i_1} \Omega_{i_2} \cdots \Omega_{i_n} \psi(\mathbf{x}, \varepsilon, \boldsymbol{\Omega}) \, d\boldsymbol{\Omega}$$

- simple linear model for the closure of the distribution function

$$\psi^{(lin)}(\boldsymbol{x}, \varepsilon, \boldsymbol{\Omega}) = \sum_{l=0}^{N} \psi^{(l)}_{i_1 i_2 \cdots i_l}(\varepsilon, \boldsymbol{x}) \, \Omega_{\langle i_1} \Omega_{i_2} \cdots \Omega_{i_l \rangle} = \sum_{l=0}^{N} \sum_{k=-l}^{l} \psi^{(l)}_k(\varepsilon, \boldsymbol{x}) \, Y_{k,l}(\boldsymbol{\Omega})$$

- example equations with two variables ($N = 1$) - the P_1-model

$$-\frac{\partial}{\partial \varepsilon}\left(S(\mathbf{x}, \varepsilon)\, \psi^{(0)}(\mathbf{x}, \varepsilon)\right) + \frac{\partial \psi_i^{(1)}(\mathbf{x}, \varepsilon)}{\partial x_i} = 0$$

$$-\frac{\partial}{\partial \varepsilon}\left(S(\mathbf{x}, \varepsilon)\, \psi_i^{(1)}(\mathbf{x}, \varepsilon)\right) + \frac{1}{3}\frac{\partial \psi^{(0)}(\mathbf{x}, \varepsilon)}{\partial x_i} = -T(\mathbf{x}, \varepsilon)\, \psi_i^{(1)}(\mathbf{x}, \varepsilon)$$

- transport coefficient follows from scattering cross sections

$$T(\boldsymbol{x}, \varepsilon) = \sigma_{\mathrm{tot}}^{(\mathrm{loss})}(\boldsymbol{x}, \varepsilon) + \int_{-1}^{1} \sigma^{(\mathrm{CSD})}(\boldsymbol{x}, \varepsilon, \mu) d\mu$$

Hierarchy of P_N-Models

- for better accuracy typically $N > 1$ is used, with variable vector $\underline{\psi} = \left\{ \psi_k^{(l)} \,,\, l \leq N, |k| \leq l \right\}$
- P_N-equations can be written as generic system $-\partial_\varepsilon \left(S\underline{\psi} \right) + \underline{\underline{A}}^{(x)} \partial_x \underline{\psi} + \underline{\underline{A}}^{(y)} \partial_y \underline{\psi} + \underline{\underline{A}}^{(z)} \partial_z \underline{\psi} = \underline{\underline{T}}\, \underline{\psi}$
- stopping power and transport coefficient matrix are related to underlying density fields of the elements

$$S\left(\varepsilon, \boldsymbol{x}\right) = \sum_{i=1}^{n_e} \rho_i(\boldsymbol{x}) S_i(\varepsilon)\,, \qquad \underline{\underline{T}}\left(\varepsilon, \boldsymbol{x}\right) = \sum_{i=1}^{n_e} \rho_i(\boldsymbol{x}) \underline{\underline{Q}}^{(i)}(\varepsilon)$$

- system matrices $\underline{\underline{A}}^{(x,y,z)}$ describe wave propagation
- matrices $\underline{\underline{A}}^{(x,y,z)}$, $\underline{\underline{T}}$ are sparsely occupied
- the hierarchy of models comes in a cascading format
- system matrices for large N are computer-generated
- numerically solved with specialized finite difference methods (StarMap algorithm)

$\underline{\underline{A}}^{(x)} =$

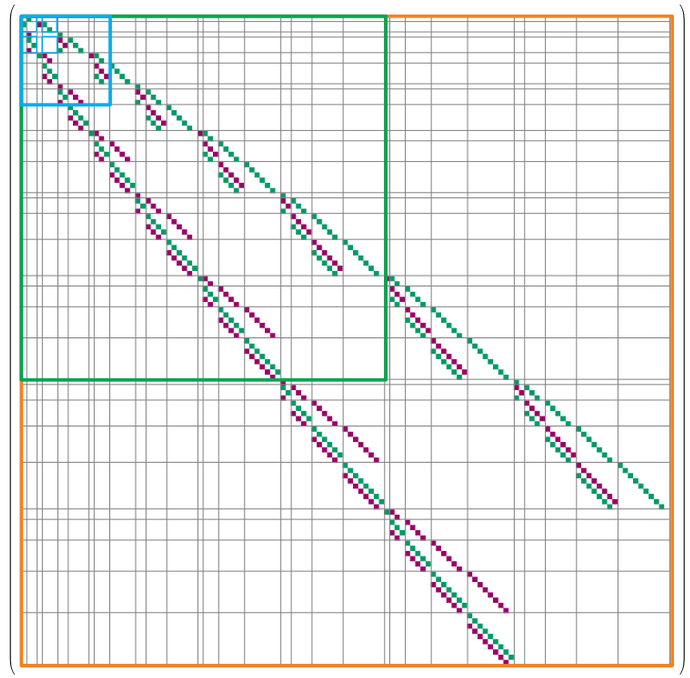

Electron Probe Micro-Analysis

- goal: find chemical composition in a material sample, e.g, metallic alloy, geological sample
- n_e chemical elements: $\mathcal{A}_1, \mathcal{A}_2, \cdots \mathcal{A}_{n_e}$, mass densities: $\rho_1, \rho_2, \cdots, \rho_{n_e}$
- intensity measurements: $I_1^{(exp)}, I_2^{(exp)}, \cdots I_{n_e}^{(exp)}$ depending on the chemical composition

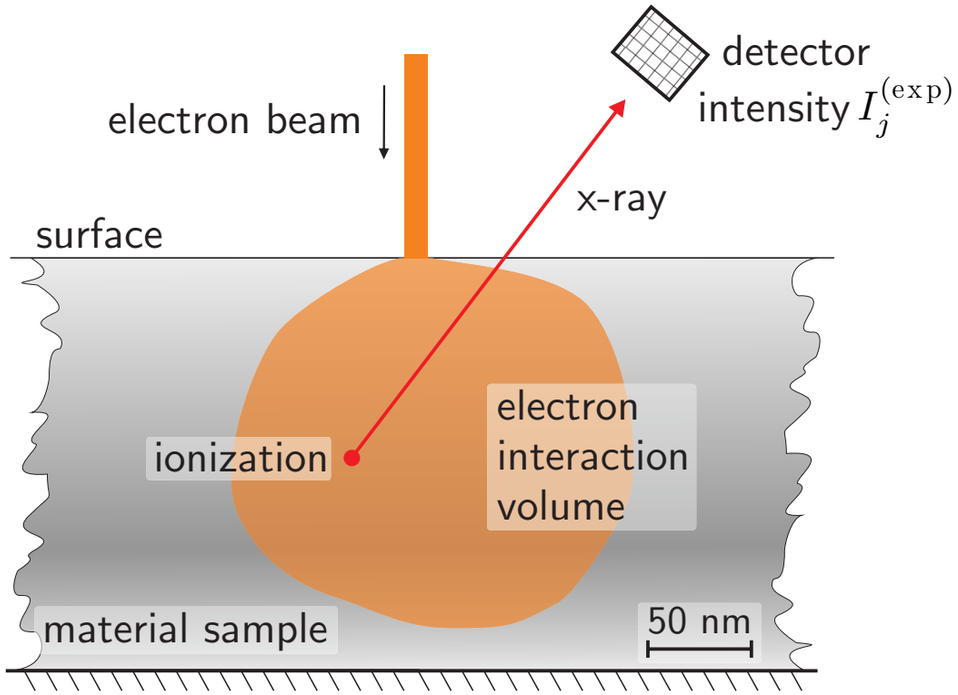

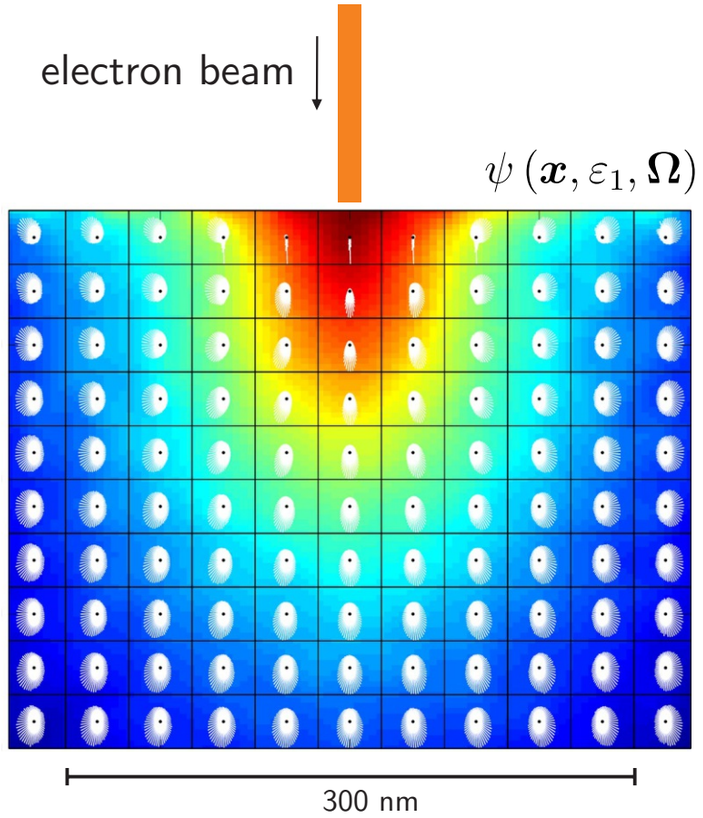

Forward Problem for EPMA Intensities

- electron fluence gives rise to ionization, this generates x-rays, which will be attenuated while propagating to the detector

$$I_j^{(model)}[\rho] = \int_{R^3} \underbrace{e^{-\int_{d(\boldsymbol{x})} \mu_{(Z,j)}(z;\rho)\mathrm{d}z}}_{\textit{attenuation}} \underbrace{\frac{\rho_z(\boldsymbol{x})}{A_Z}}_{\textit{number atoms}} \underbrace{\int_0^\infty \sigma_{(Z,j)}(\epsilon)\psi^{(0)}(\varepsilon, \boldsymbol{x}; \rho)\mathrm{d}\varepsilon}_{\textit{ionization } \phi[\psi^{(0)}](\boldsymbol{x})} \mathrm{d}\boldsymbol{x}$$

- ionization depends on the moment $\psi^{(0)}(\varepsilon, \boldsymbol{x}) = \int_{\mathcal{S}^2} \psi(\boldsymbol{x}, \varepsilon, \boldsymbol{\Omega})\, d\boldsymbol{\Omega}$
- P_N-theories can be viewed as efficient model reduction to specifically compute $\psi^{(0)}(\varepsilon, \boldsymbol{x})$
- electron beam position and energy enter as boundary conditions for the P_N-system
- density fields enter as coefficients of the P_N-system

Classical EPMA Forward Models

- deterministic/noise-free diffusion forward models also have been considered, see Brown & Ogilvie (1966)

Matrix Correction Methods

- classical approach developed in 1950's, still widely used, see, e.g., Pouchou (1993), Goldstein (2003)
- take into account empirical atomic number / absorption / flourescence corrections
- assumes homogeneous material
- resolution restricted to electron interaction volume

Monte-Carlo Particle Method

- trace individual electrons travelling through the material, effects of collision determined by random variables
- various code packages exits, e.g. DTSA-II, NeXL, see Ritchie (2009,2022), PENELOPE/PENEPMA, see Salvat (1995-), CASINO/MC X-Ray, see Gauvin (2009)
- many physical aspects can be modeled accurately, extensively validated
- computationally very expensive, exhibits statistical noise

Ionizations in EPMA Experiments (homogeneous)

- validate homogenous ionizations $\phi(\rho z)$ obtained from classical models, Monte-Carlo and P_n model
- use deterministic P_N moment model with $N = 21$ for high resolution

- pure copper, K-L2 transition
- beam energies 15keV and 12keV

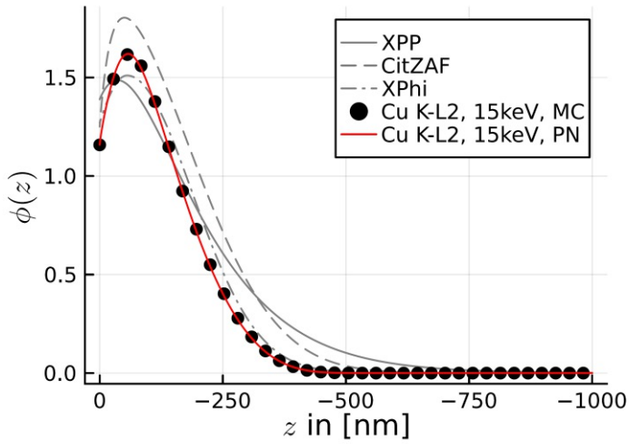

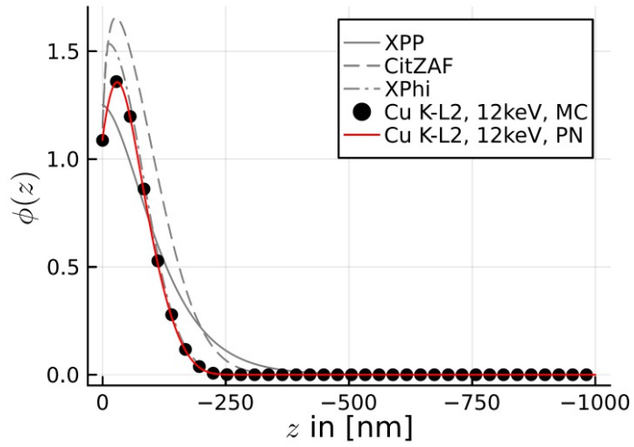

- pure chromium, K-L2 transition
- beam energies 15keV and 12keV

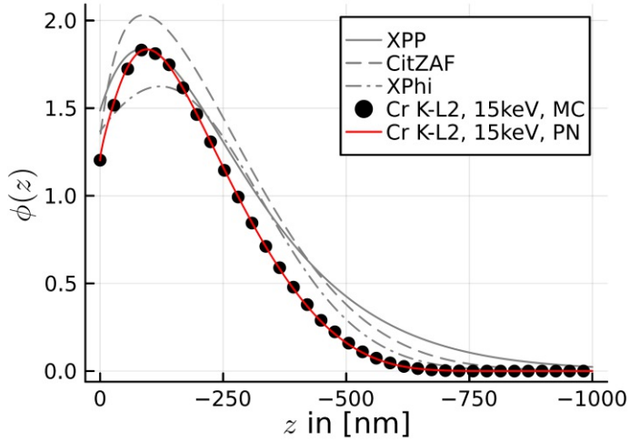

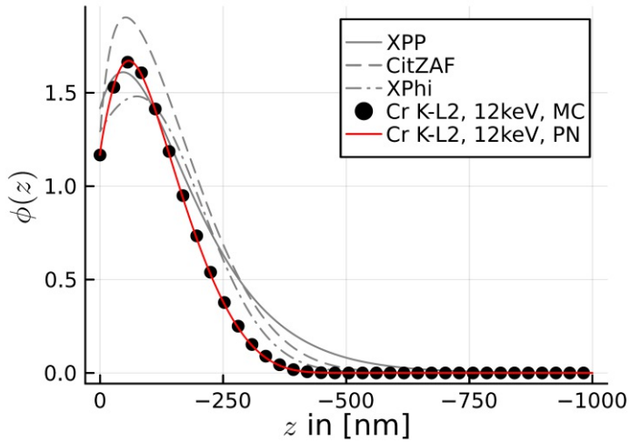

Ionizations in EPMA Experiments (horizontal layers)

- compare ionization $\phi(\rho z)$ for horizontal layer setup, obtained from Monte-Carlo and P_N
- essentially 1D situation allows very fast computational implementation
- use different levels $N = 3,9,21$ to demonstrate model convergence
- for this setup the P_9 model has sufficient accuracy

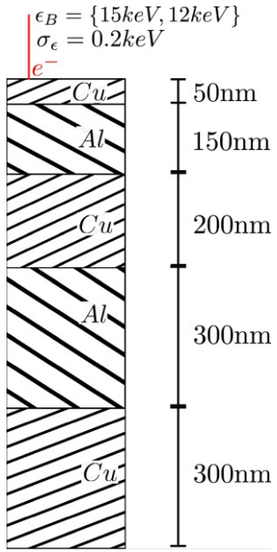

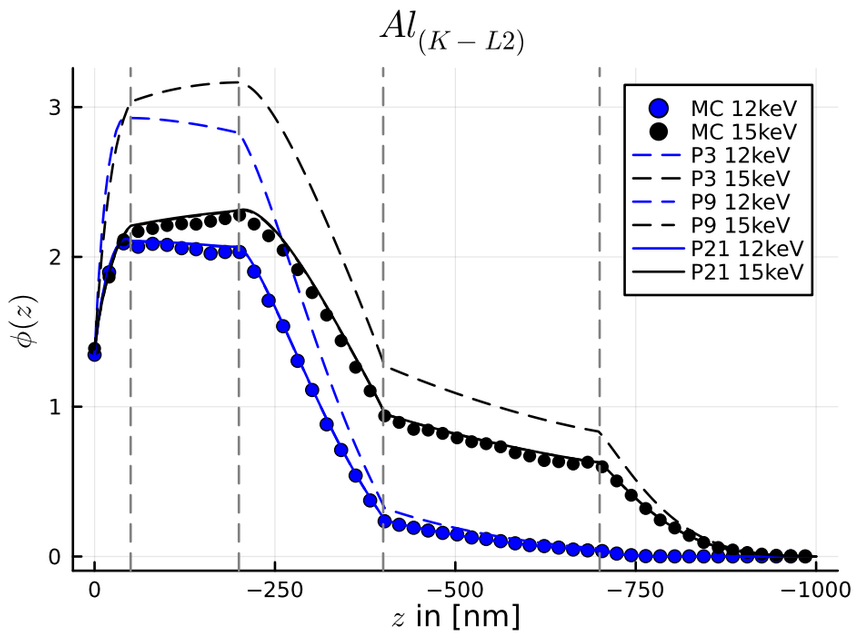

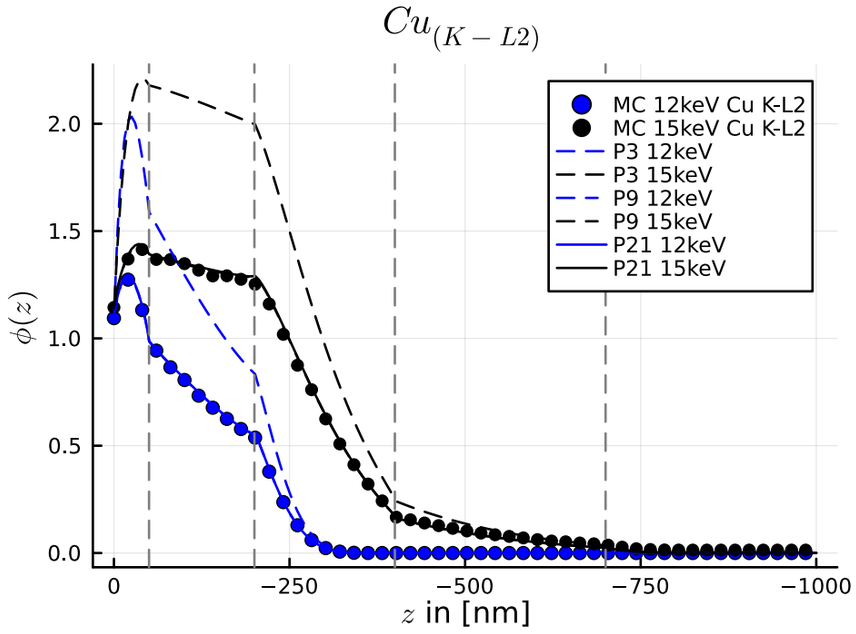

Ionizations in EPMA Experiments (vertical interface)

- compare energy distributions of various P_N models with MC for an interface sample

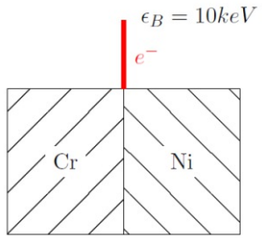

- filtering techniques FP_N allow to speed-up model convergence

- P_N is computationally much faster than MC in principle

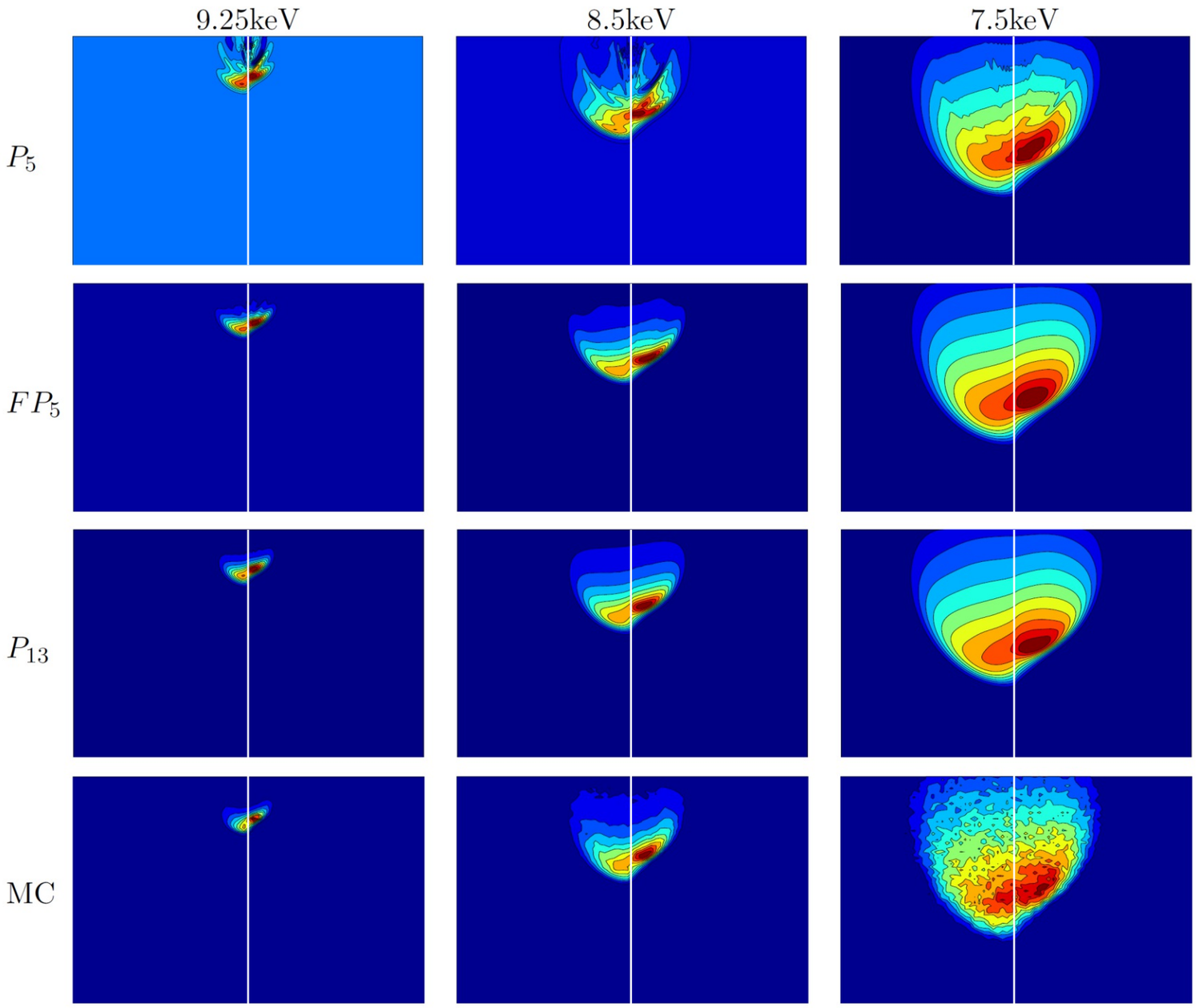

Ionizations in EPMA Experiments (2D case with 2x2 block)

- compare energy distributions of various P_N models with MC for an material composite (Al, Ag, Au)

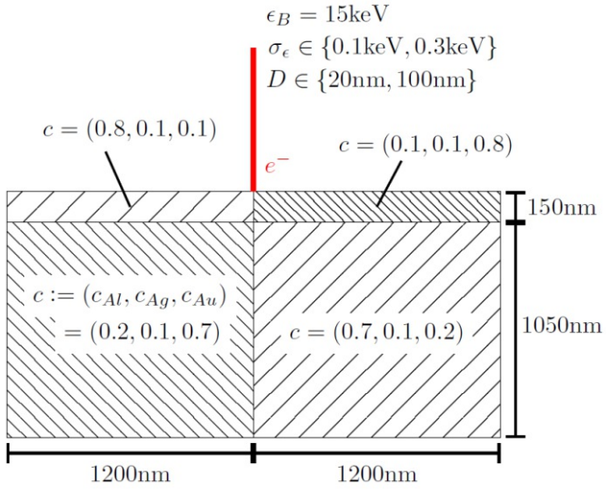

- P_{21} and P_{13} are essentially in perfect agreement
- hence, P_{13} has sufficient accuracy

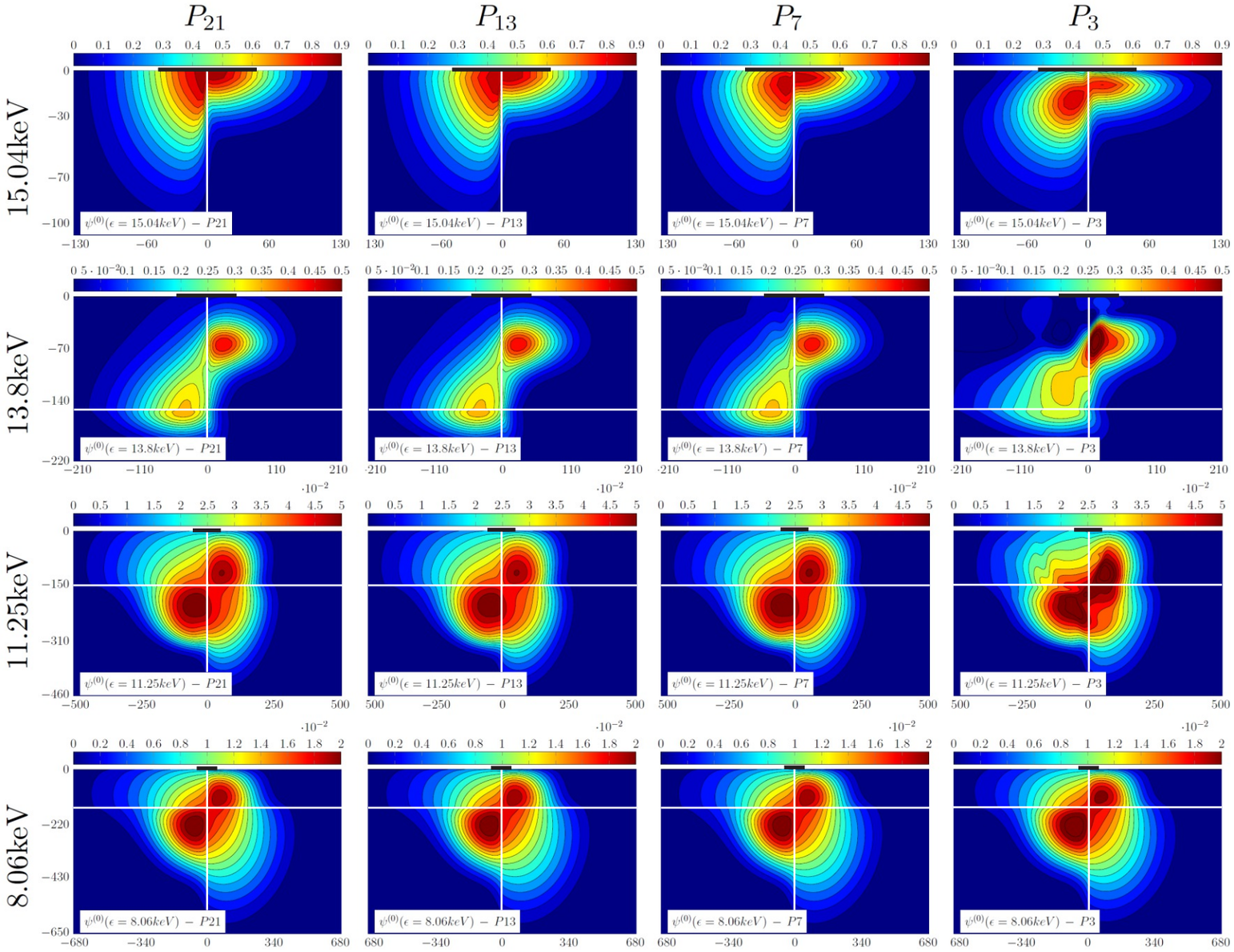

P_9-Fluence Computations in 3D

- homogeneuous copper-nickel material with beam energy 12 ± 0.3keV
- animation shows successive energy levels, with each densities normalized to their maximal values

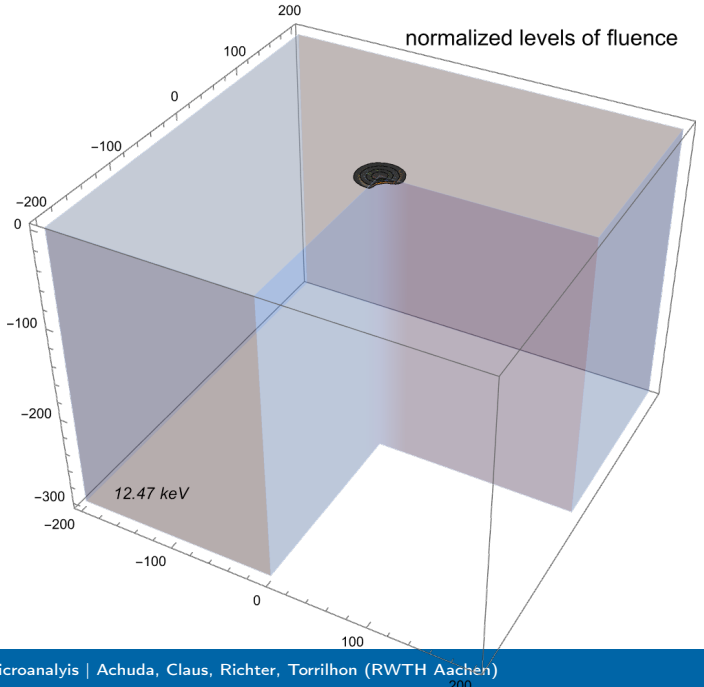

The Inverse Problem of EPMA

- strong heterogeneities and sub-scale resolution requires multiple overlapping measurements
- mass densities are fields depending on position x

$$\rho_1(\boldsymbol{x}), \rho_2(\boldsymbol{x}), \cdots, \rho_{n_e}(\boldsymbol{x})$$

- multiple intensity measurements $k = 1, 2, \ldots$ from different beam positions, possibly different energies

$$\left\{ I_{j,k}^{(exp)} \right\}_{\substack{j=1,\cdots n_e \\ k=1,2,\ldots}}$$

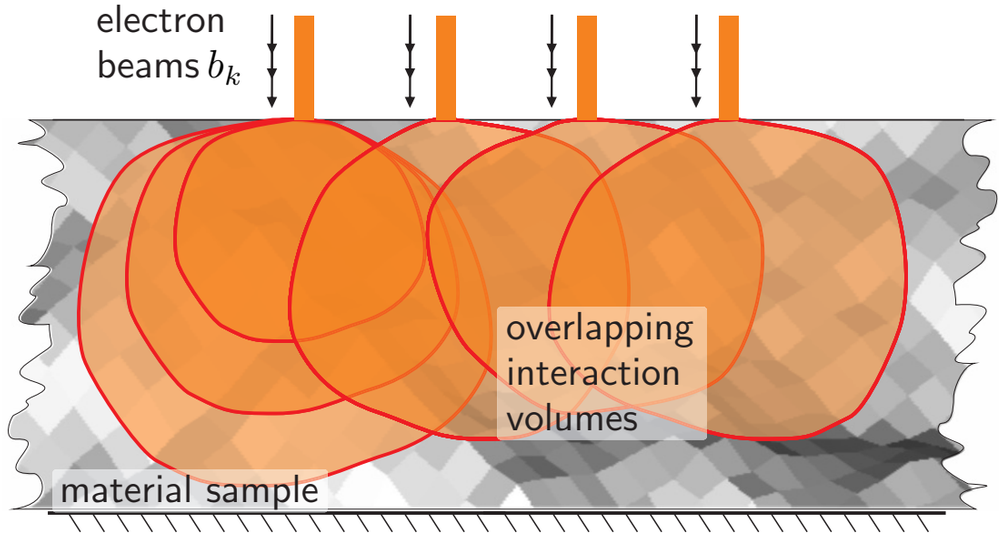

- the density field influences many measurements (convolution), yielding a nonlinear inverse problem

$$\mathcal{Y}[\rho] = \sum_{j,k} \left(I_{j,k}^{(exp)} - I_{j,k}^{(model)}[\rho(\boldsymbol{x})] \right)^2 \rightarrow min$$

- gradient-based optimization methods require
  - a representation of the density field as a function of finite parameters
  - an iteration that goes through density fields $\rho^{(0)}, \rho^{(1)}, \rho^{(2)}, \cdots$ starting from an initial guess
  - computation of a search direction based on the derivative of the target function $\frac{\partial \mathcal{Y}[\rho]}{\partial \rho}$

Density Representations

- a general density field $\rho_i : \mathbb{R}^d \to \mathbb{R}, \boldsymbol{x} \mapsto \rho(\boldsymbol{x})$ contains infinitely many degrees of freedom
  ↯ impossible to reconstruct from finite measurement data
- regularization of the inverse problem assumes the density field to be given by a finite set of parameter $\boldsymbol{p} \in \mathbb{R}^{n_p}$
- density becomes a mapping of space controlled by these parameters $\rho_i(\boldsymbol{x}; \boldsymbol{p})$
- many different representations are possible, depending on the situation, must be chosen a-priori

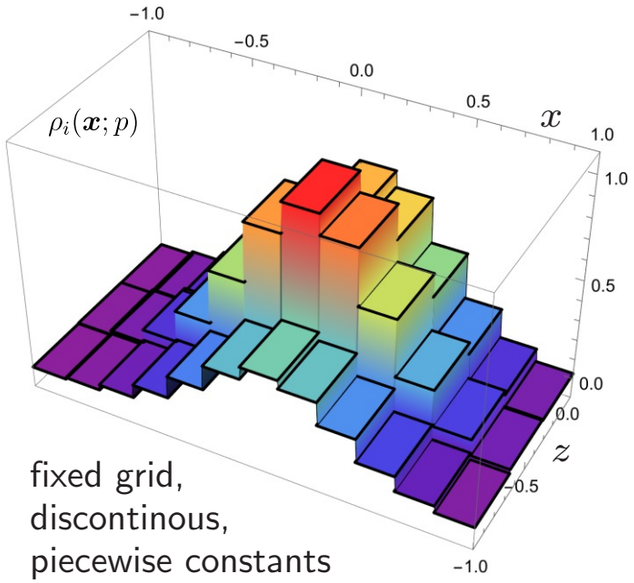

fixed grid,
discontinous,
piecewise constants
3×12=36 parameters

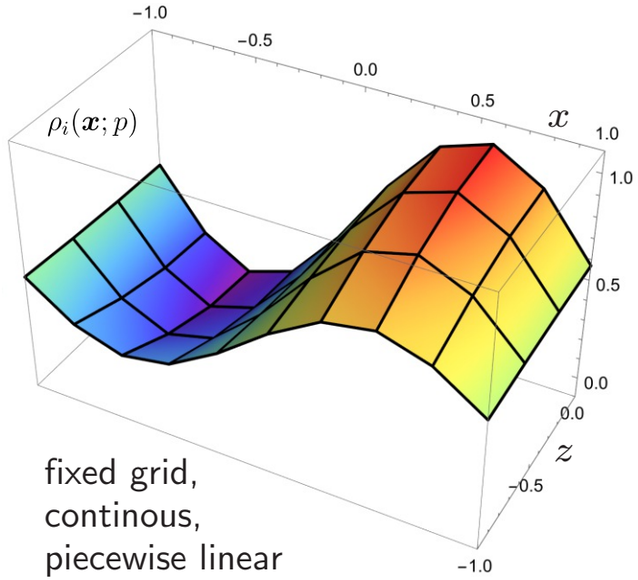

fixed grid,
continous,
piecewise linear
4×10=40 parameters

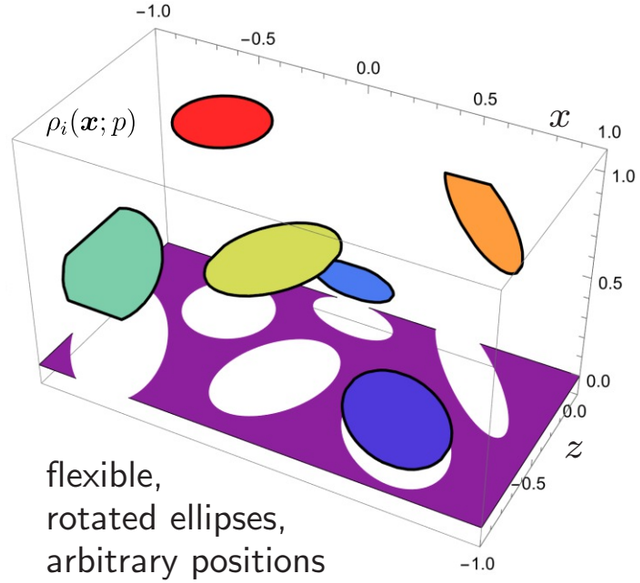

flexible,
rotated ellipses,
arbitrary positions
6×6+1=37 parameters

Differentiation Dependency Graph for Continous Adjoint

- adjoints can be viewed as backward derivatives to accelerate algorithmic differentiation
- used to compute the implicit dependence of the energy distribution on the density through the solution of the P_N system
- energy-discrete intensity $$I_{j,k}^{(model)}[\rho] = \int_{R^3} \underbrace{e^{-\int_{d(\boldsymbol{x})} \mu_{(Z,j)}(z;\rho)\mathrm{d}z}}_{\textit{attenuation}} \underbrace{\frac{\rho_z(\boldsymbol{x})}{A_Z}}_{\textit{number atoms}} \underbrace{\sum_{\varepsilon=\varepsilon_{init}}^{\varepsilon_{cut}} \sigma_{(Z,j)}(\varepsilon)\psi^{(0)}(\varepsilon,\boldsymbol{x};\rho)}_{\textit{ionization } \phi[\psi^{(0)}](\boldsymbol{x})} \mathrm{d}\boldsymbol{x}$$

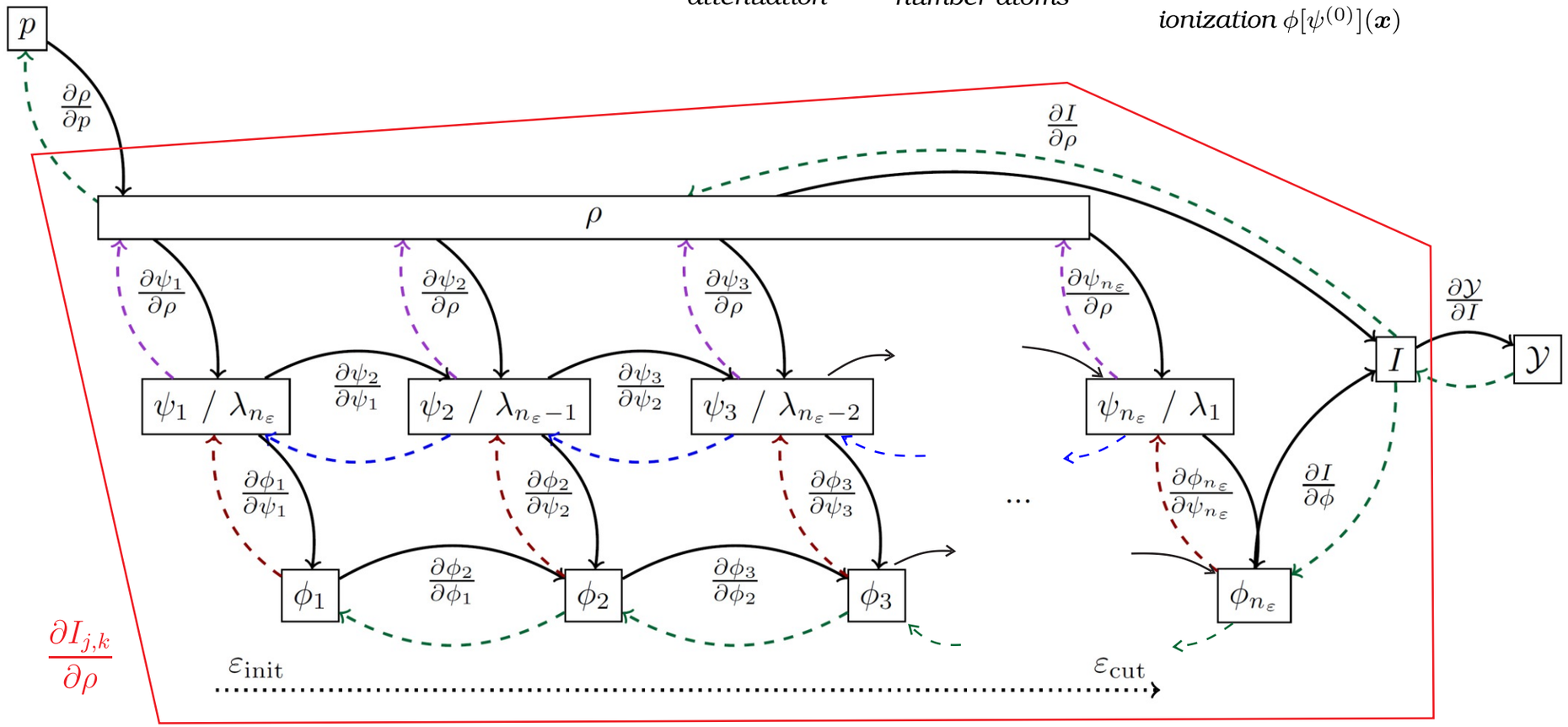

Reconstruction of 1D Interfaces

- consider two interface problems with two different density representations
- interface problems: (i) sharp interface with two plateaus, (ii) smooth interface with three plateaus
- representations: (A) piecewise constant, discontinuous, (B) piecewise linear, continuous

- Fe-layer covering a Ni-substrate
- measurements synthezised from hidden truth
- in total, data from 20 k-ratios

domain	$(-500\,\text{nm}, 0\,\text{nm})$
discretization	$n_x = 100$
energies	$(7.0\text{keV}, 15.5\text{keV})$
approximation P_N	$N = 9$
beam ϵ	$\{9, 10.5, 12, 13.5, 15\}\,\text{keV}$
beam width σ_ϵ	$0.1\,\text{keV}$
elements/x-rays	$Ni : KL_2, KL_3$
	$Fe : KL_2, KL_3$

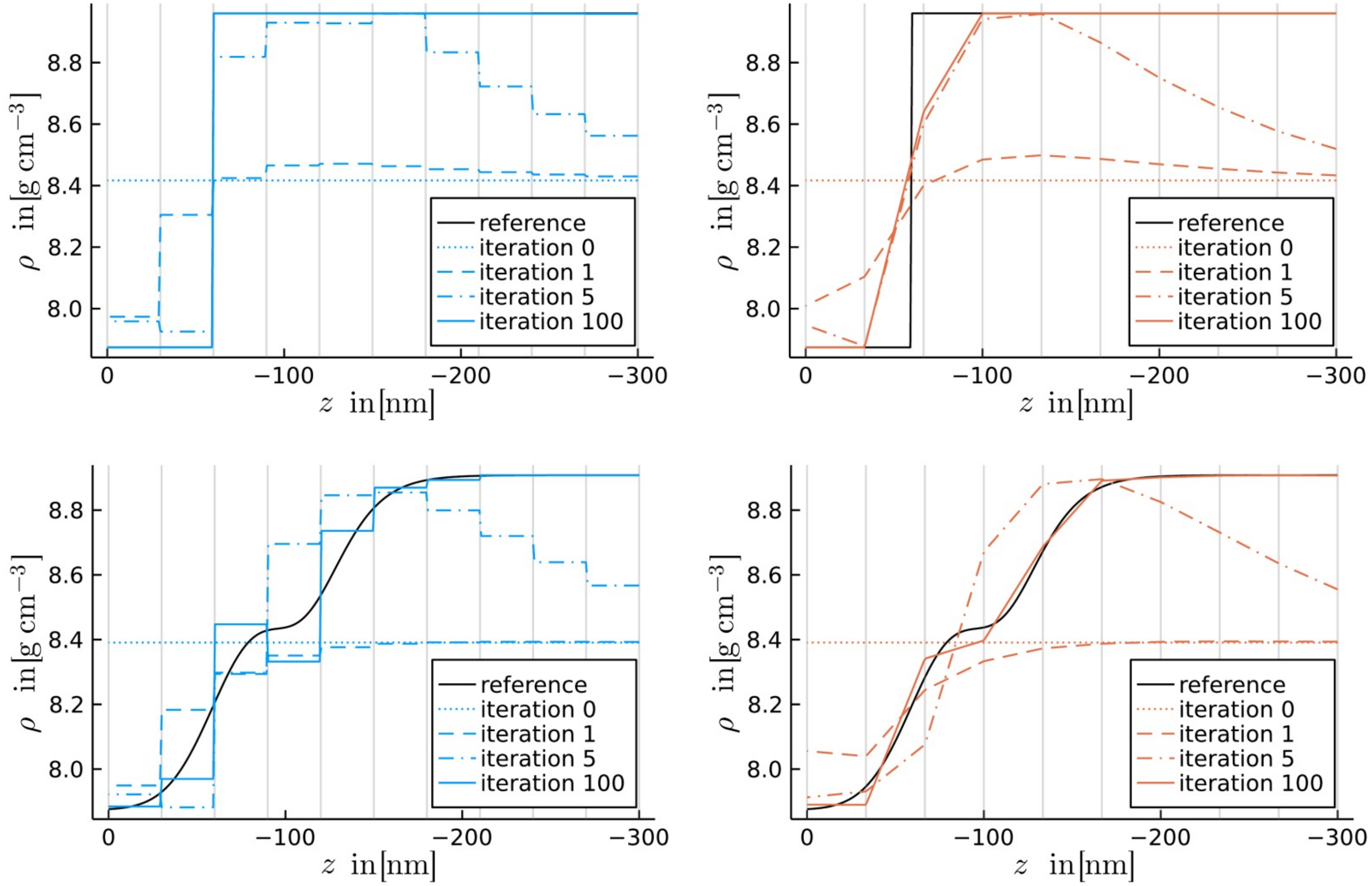

Reconstruction of a Material Inclusion in 2D

- virtually create a sample with material inclusion of ellipsoidal shape, as hidden truth
- setup:

domain $\mathfrak{S}$	$(-300\text{nm}, 0\text{nm}) \times (-150\text{nm}, 150\text{nm})$ $(n_x, n_y) = (80, 80)$
energies $[\epsilon_{\text{cut}}, \epsilon_{\text{min}}]$	$(7.0\text{keV}, 12.5\text{keV})$
approximation order P_N	$N = 9$
beam $\mu_\epsilon, \sigma_\epsilon$	12keV, 0.2keV
beam μ_x, σ_x	$(0, \{-50, -25, 0, 25, 50\})\text{nm}$, 20nm
beam μ_Ω, κ	$[-1, 0]$, 10
elements/x-rays	$(Cu, K-L_2)$, $(Cu, K-L_3)$, $(Fe, K-L_2)$ and $(Fe, K-L_3)$
standard materials	$(Cu, K-L_*) : (1.0Cu, 0.0Fe)$, $(Fe, K-L_*) : (0.0Cu, 1.0Fe)$

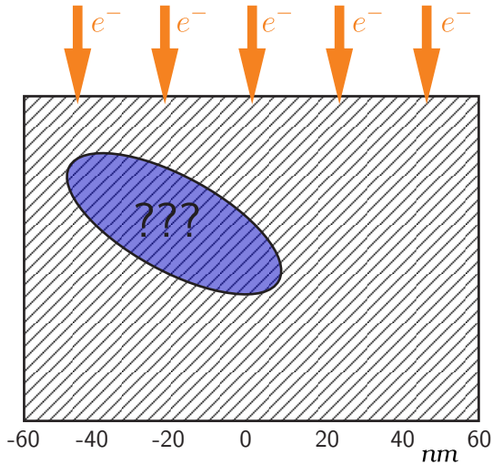

- synthesize k-ratio data from virtual experiment, no noise, computed by P_N-model

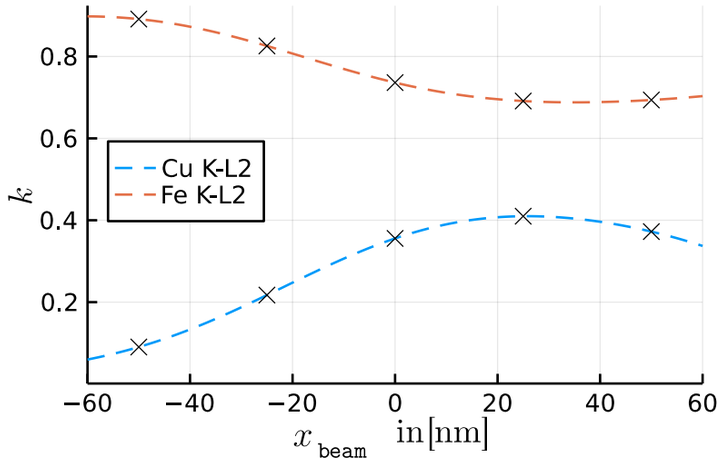

Reconstruction of a Material Inclusion - Iteration Visualization

- assuming an ellipse shape as density field representation
- animation shows successive iterations of the optimization of the intensities wrt the measurements

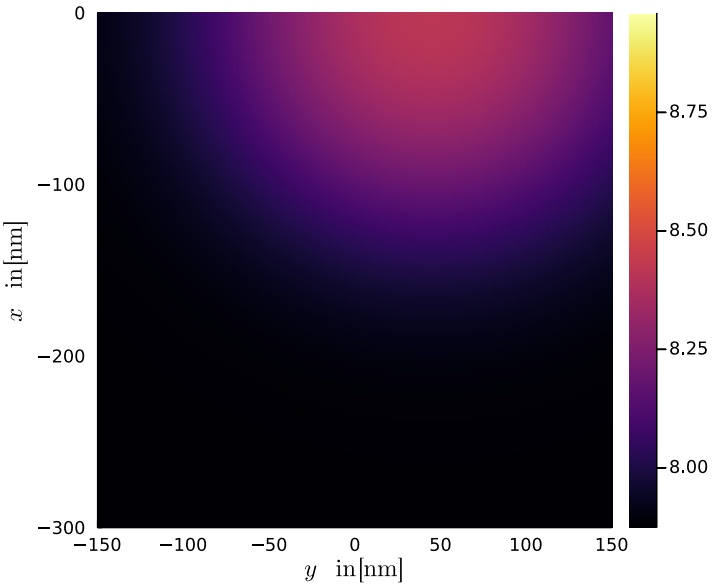

Reconstruction of a Material Inclusion - Iteration Visualization

- assuming an ellipse shape as density field representation
- animation shows successive iterations of the optimization of the intensities wrt the measurements

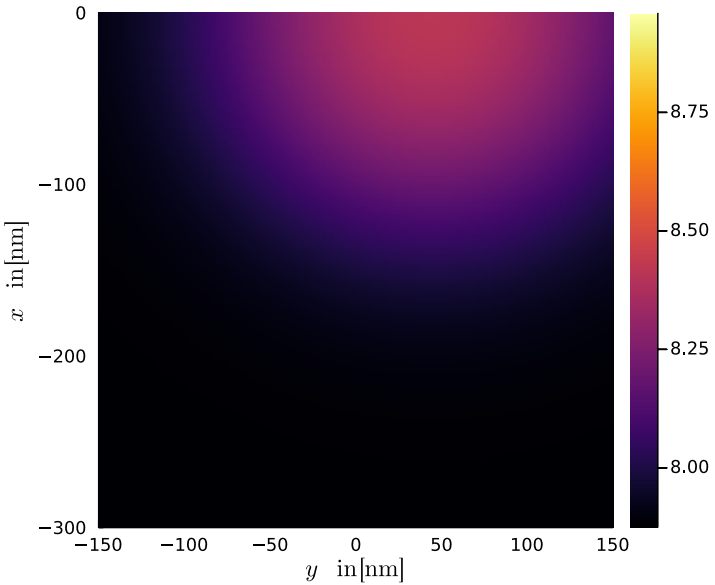

Reconstruction of a Material Inclusion - Iteration Visualization

- assuming an ellipse shape as density field representation
- animation shows successive iterations of the optimization of the intensities wrt the measurements

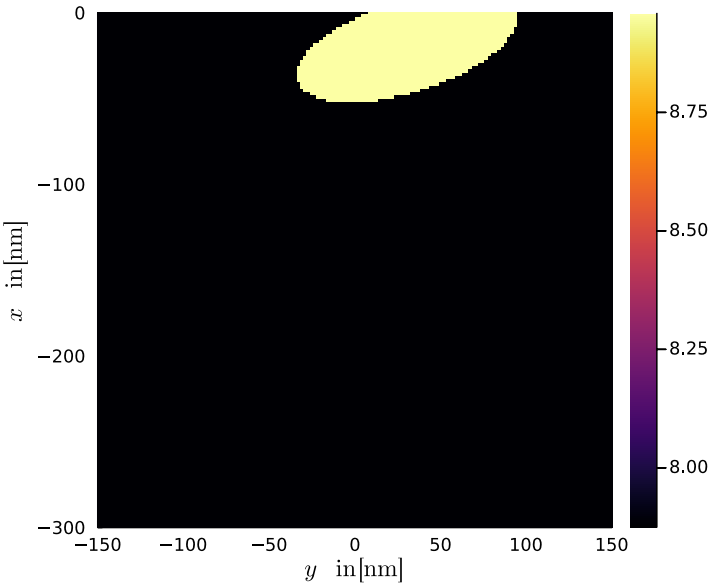

Conclusion and Outlook

- **deterministic moment equations** for electron transfer are effective for electron micro-beam experiments
- **inverse problem** can be solved using efficient optimization techniques for partial differential equations
- **more validation** based on x-ray emissions required with Monte-Carlo simulations and experiments
- **uncertainty quantification and high-performance computing** must be considered in the future
- see also:
  posters by Gaurav Achuda and Tamme Claus
- comments and feedback are very welcome